mathematics

Article

Supply Restoration in Active Distribution Networks Based on Soft Open Points with Embedded *DC* Microgrids

Irina I. Picioroaga, Andrei M. Tudose *, Dorian O. Sidea and Constantin Bulac

Department of Electrical Power Systems, University "Politehnica" of Bucharest, 060042 Bucharest, Romania; irina.picioroaga@upb.ro (I.I.P.); dorian.sidea@upb.ro (D.O.S.); constantin.bulac@upb.ro (C.B.)
* Correspondence: andrei.tudose1604@upb.ro

Abstract: As disturbances due to natural disasters or man-made attacks intensify awareness regarding power systems' resilience enhancement, the scientific community concentrates on exploring state-of-the-art technologies for emergency supply restoration strategies. Recent studies are increasingly focusing on the expanded flexibility of soft open points (SOPs) compared to conventional tie-switches to increase the restoration rate of critical loads; however, the potential of this novel technology is not limited to this aspect, with SOPs being used to improve the voltage level and increase the hosting capacity of renewable energy sources (RESs). This paper proposes a deterministic model for the optimal coordination of SOPs and distributed resources in an active distribution network (ADN) aiming at re-establishing the energy supply to critical loads after a prolonged interruption occurrence. At the same time, the support of *DC* microgrids with integrated RESs, embedded in SOPs, for the restoration process is explored. The efficiency of the proposed optimization model is verified based on a 24-h analysis performed on the modified IEEE 33-bus system, while considering the load and generation uncertainties as well.

Keywords: soft open point; service restoration; load uncertainty; fuzzy c-means; microgrids

check for updates

Citation: Picioroaga, I.I.; Tudose, A.M.; Sidea, D.O.; Bulac, C. Supply Restoration in Active Distribution Networks Based on Soft Open Points with Embedded *DC* Microgrids. *Mathematics* **2022**, *10*, 211. https://doi.org/10.3390/math10020211

Academic Editor: Nicu Bizon

Received: 15 December 2021
Accepted: 7 January 2022
Published: 11 January 2022

1. Introduction

Power systems' resiliency against major disasters (natural or man-made attacks) has become an essential feature for future distribution systems. Besides solving issues related to environmental protection and covering energy shortages, renewable energy sources in the form of distributed generation are increasingly integrated into strategies aiming at enhancing the reliability of the energy supply service. However, the high-penetration of these intermittent sources introduces the necessity of transitioning distribution networks to intelligent entities, capable of managing distributed generators, storage systems and loads, which leads to the emergence of a new concept, namely, active distribution networks (ADNs) [1]. The evolving ADN paradigm requires smart communication infrastructures and advanced monitoring and control technologies to ensure proper flexibility and to provide a reliable infrastructure for both the distributed energy resources and the consumers.

Modern solutions for increasing the operability and flexibility of ADNs, such as soft open points (SOPs), are receiving a higher degree of interest recently. In [2], SOPs' ability of improving distribution networks' hosting capacities of distributed generation is investigated under various objective functions (i.e., voltage profile enhancement, line utilization balancing and energy loss minimization), with the results showing that SOPs can provide up to 30% improved hosting capacity. Many studies have addressed the reconfiguration problem of ADNs in the presence of DGs and SOPs in both single and multi-objective formulations, displaying significant contributions of the SOPs regarding both technical and economic aspects, such as reducing power losses, minimizing voltage deviations and balancing electrical lines loading [3–5]. Establishing the number of SOPs and their placement in ADNs is crucial for assuring good performance during their operation.

In this regard, optimization models were proposed in the literature for SOPs' sizing and placement problems. The authors of [6] aimed at reducing the annual operation cost of the distribution network, concluding that SOPs integration may decrease the cost by up to 30%, while in [7] a stochastic model was developed to improve the three phase unbalance in distribution networks.

Over the past years the advantages of *DC* microgrids over AC microgrids have been intensely studied. Given the increasing share of *DC* powered components for residential, commercial and industrial loads and the high penetration of *DC* distributed generation units (such as photovoltaics), *DC* microgrids prove themselves the right candidates for the future development of power systems [8]. Their benefits are mainly reflected in the increased supply efficiency for *DC* loads by minimizing power losses due to a reduced number of conversion steps. The integration of *DC* renewable energy sources is facilitated as well, while the generators synchronization requirement is eliminated [9]. Authors of [10] studied the effectiveness of demand response and electric vehicle integration in isolated *DC* grids. A detailed review of the literature in planning, operation and control of the *DC* microgrids field is presented in [11], while the authors of [12] developed a control strategy for *DC* microgrids considering the presence of renewable energy sources and storage capacity. Microgrids are generally designed to reduce the energy exchanged with the utility grids, aiming at becoming self-sufficient entities. Moreover, during power outages in the utility grid caused by equipment failures, microgrids can contribute to a distribution grid's service restoration process, by increasing the generation from local energy sources and storage systems, providing the surplus generation to the ADN's loads [13]. Considering the importance of supply continuity, the restoration capabilities in the case of outages represent an essential feature of ADNs. The authors of [14] proposed a heuristic strategy to identify the optimal path in a distribution grid in order to restore the supply to critical loads through microgrids participation. *DC* microgrids access to the main distribution grid can be facilitated if SOPs are used within the network, as the *DC* microgrid can be connected to the *DC* bus of the SOP using a *DC*–*DC* converter. In addition to active power flow control and reactive power regulation, the SOP-microgrid aggregation may ensure new functions, such as energy storage, through storage devices installed in microgrids [15].

The operation of distribution networks is governed by uncertainties, introduced by the stochastic nature of renewable energy sources, as well as the load. The main techniques employed within the literature in modelling uncertainties include probabilistic and possibilistic techniques, stochastic and robust optimization [16]. A scenario selection method based on Monte Carlo simulations is proposed in [17] to deal with the uncertainties of load, wind and solar irradiance to solve the problem of network expansion, while a fuzzy uncertainty technique is investigated in [18] to build a decision-making tool for transmission systems planning.

In this paper, a methodology based on Mixed Integer Second-Order Cone Programming (MISOCP) is developed in order to restore the supply after a line fault occurrence in the distribution network, based on an SOP-microgrid coordination, while prioritizing important loads. To validate the effectiveness of the proposed model, two schemes are investigated for comparative analysis, including a supply restoration strategy based on the conventional approach including reconfiguration and tie switches and the proposed supply restoration methodology. The benefits of SOPs and *DC* microgrids support for the restoration process are assessed for a modified IEEE-33 bus test system, considering a 24-h analysis. Uncertainties from various sources (i.e., multiple types of loads, wind and solar generation) are modelled with the Fuzzy c–means clustering technique. Therefore, the contributions of our paper can be highlighted as follows:

1. Developing a supply restoration strategy based on MISOCP for ADNs, including SOPs and *DC* microgrids connected at the *DC* interface of a SOP,
2. Extracting the most representative scenarios from the available load and generation data through the Fuzzy c-means algorithm,
3. Applying the previously mentioned optimization model on a modified IEEE 33-bus system,

4. Evaluating the benefits provided by SOPs and microgrids participation on the supply restoration strategy.

The rest of the paper is organized as follows: Section 2 discusses the soft open points principle and the integration of *DC* microgrids. In Section 3, the mathematical formulation of the optimization model is discussed, alongside the uncertainty modelling procedure. Section 4 presents the distribution system used in the case study, namely, the modified IEEE 33-bus system, and the results of Fuzzy c–means clustering for the load and generation scenarios, while the restoration results are analyzed in Section 5. Finally, the conclusions are outlined in Section 6.

2. Soft Open Point

A soft open point is a novel power electronics-based equipment, proposed in [19] and introduced in distribution networks as an alternative to tie switches, known as normally open points (NOP). Presently, three different topology versions are proposed for SOPs: two voltage source converters (VSC) disposed in a back-to-back connection, a unified power flow controller which consists of a series-connected VSC and a shunt-connected VSC, and a static synchronous series compensator consisting of a series-connected VSC [20]. The SOP topology considered in this paper consists of two back-to-back voltage source converters, as shown in Figure 1. The two three-phased VSC converters, based on insulated gate bipolar transistors (IGBT) with pulse-width modulation (PWM) control are connected on the *DC* side through a capacitor, *C*. Each converter is then connected to the AC distribution network through a series filter, represented by the inductances *L*.

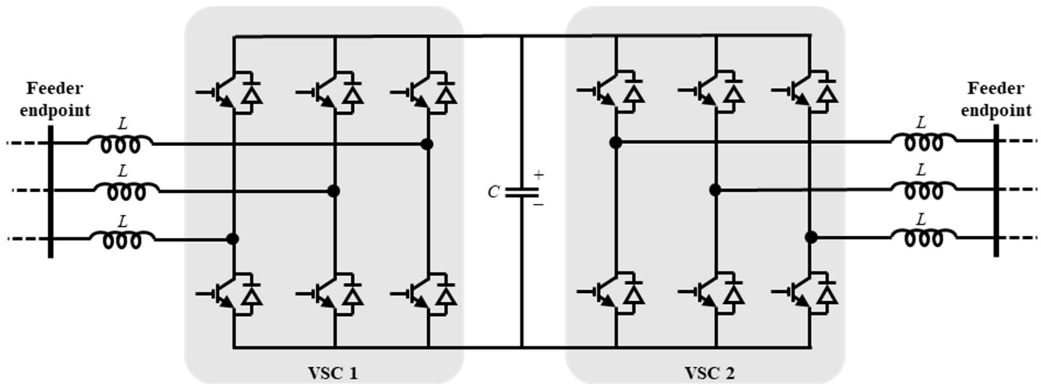

Figure 1. Soft open point configuration.

The two voltage source converters provide SOPs an increased versatility and extensive control capabilities under both normal and abnormal operating conditions. Firstly, as each VSC converter is capable of independent reactive power control (Figure 2), SOPs contribute to the reactive power compensation and voltage regulation for each feeder (Figure 3). Secondly, the active power flow between the two VSC converters, assured by the *DC* link, enable SOPs to control the active power flow and ensure load balancing capabilities [21]. The VSC technology also provides relatively instantaneous voltage control characterized by a few milliseconds' response time, granting transient control and power oscillations dumping capabilities for the SOPs. Moreover, SOPs can isolate the faults or disturbances occurring on a feeder connected to a VSC converter from extending to the feeder of the other side of the SOP [22]. Finally, when the loads connected to one VSC are unsupplied, the SOP can provide support in the network restoration by assuring an active power supply from the other VSC. Consequently, due to their versatility, SOPs are suitable for various applications such as: voltage profile improvement, active power losses reduction [3], integration of distributed energy sources [23], transient control [24], and fault isolation [25], etc.

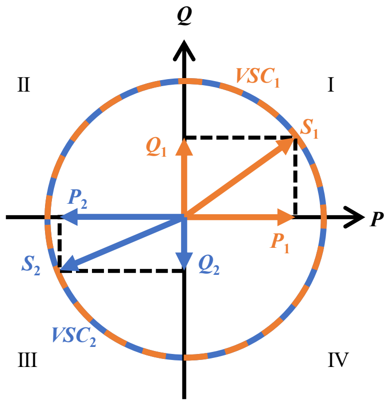

Figure 2. Operating region of the soft open point.

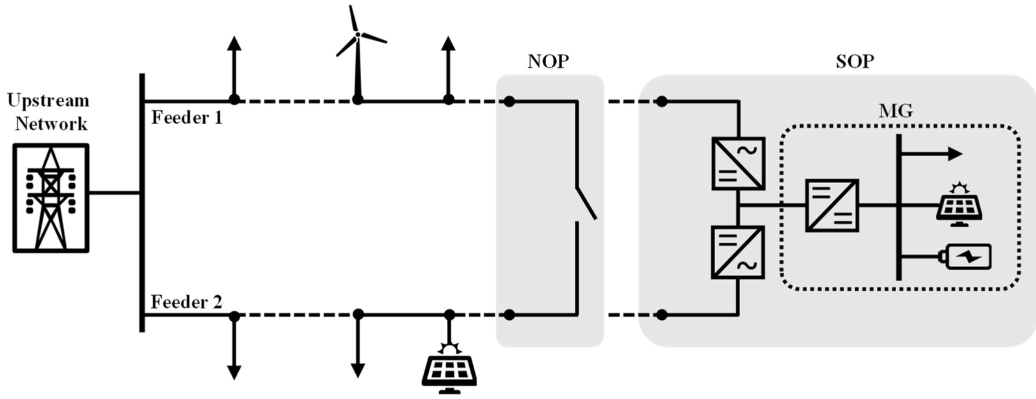

Figure 3. Soft open point and *DC* microgrid integration in the active distribution network.

Furthermore, recent research has extended the SOP capabilities by connecting energy storage system (ESS) devices on the *DC* side through a *DC*/*DC* converter [26]. The ESS device allows the SOP to supply loads during periods characterized by high energy prices using the energy previously stored during periods with low energy prices or high renewable generation. In this manner, the SOP and ESS have the capability to provide an important operating costs reduction. In this study, the SOP flexibility is further explored by integrating *DC*−microgrids through the *DC* connection, allowing them to participate in the supply restoration process. Additional to RESs, ESSs are among the typical components of *DC* microgrids, which may contribute to the demand and generation shift in time, in order to reduce the distribution network loading. Consequently, in fault conditions, the coordination between microgrids and ADNs may lead to a higher ratio of the recovered load.

Considering the increasing interest in *DC* microgrids, an efficient method to connect them in the public AC distribution grid would consist in connecting the microgrid through a *DC*/*DC* converter to the *DC* side of a SOP. Figure 3 depicts the proposed SOP with an embedded *DC* microgrid architecture integrated in the ADN.

3. Problem Formulation

In this section, the uncertainty modelling for fluctuating loads and DG outputs is introduced at first, followed by the proposed optimization model for solving the supply restoration problem.

3.1. Uncertainty Modelling

Modelling the uncertainties occurring in active distribution networks represents a challenging task, as there are various sources of uncertainty (i.e., load and generation from renewable sources). The uncertainties regarding various type of loads (i.e., residential, commercial and industrial) are considered in this paper, as well as the uncertainties of photovoltaics (PV) and wind generation. Therefore, modelling uncertainties through classical methods, such as Monte Carlo simulations or scenario-based analysis, may require an exceedingly high number of analyzed scenarios, leading to a poor computational efficiency [27]. Assuming the availability of historical data, clustering techniques may be employed to achieve an improvement in the computational time.

Clustering represents a machine learning technique based on unsupervised learning, which explores the similarities between data and identifies the best partitioning of data into clusters. The centers of the clusters depict the most representative scenarios for the given dataset and the analysis is further conducted on the resulted cluster centers. The Fuzzy c-means (FCM) algorithm (Algorithm 1) represents one of the most frequently used clustering techniques in the literature, as it is easy to implement and assures a fast convergence [28–30]. Moreover, the FCM algorithm provides a higher flexibility compared to k-means, as each data point is simultaneously assigned to each cluster with a different degree of memberships. Considering C as the predetermined number of clusters, the FCM algorithm minimizes the following objective function:

$$J = \sum_{i=1}^{N} \sum_{j=1}^{C} \mu_{ij}^{m} \|x_i - c_j\|^2 \tag{1}$$

where N represents the number of data points, μ_{ij} is the degree of membership of data point x_i to cluster j, m is the fuzzy parameter and c_j is the center of cluster j. The notation $\|x_i - c_j\|$ implies the Euclidean distance between data point x_i and cluster center c_j. Parameter m is set to 1.5 in this paper.

The positions of clusters' centers are determined according to Equation (2):

$$c_j = \frac{\sum_{i=1}^{N} \mu_{ij}^{m} x_i}{\sum_{i=1}^{N} \mu_{ij}^{m}} \quad \forall j = 1 \ldots N \tag{2}$$

For each data point, the degree of membership to each cluster is updated using the following equation:

$$\mu_{ij} = \frac{1}{\sum_{k=1}^{N} \left(\frac{\|x_i - c_j\|}{\|x_i - c_k\|} \right)^{\frac{2}{m-1}}} \quad \forall i = 1 \ldots N, \forall j = 1 \ldots C \tag{3}$$

The detailed iterative process of the FCM algorithm is described below.

Algorithm 1. Pseudocode of Fuzzy c-means clustering method

Input: Number of clusters C, a set of N data points $x_1, x_2, \ldots, x_N$, the fuzzy parameter m and the maximum number of iterations $iter_{max}$.
Output: Positions of cluster centers $c_1, c_2, \ldots, c_C$.

1. For each data point $i = 1 \ldots N$ and cluster $j = 1 \ldots C$, randomly initialize the degree of membership μ_{ij}.
2. Initialize number of iterations $iter = 0$.
3. For each cluster $j = 1 \ldots C$ update the cluster center using Equation (2).
4. For each data point $i = 1 \ldots N$ and cluster $j = 1 \ldots C$, update the degree of membership μ_{ij} using Equation (3).
5. Compute the objective function J described by Equation (1).
6. Repeat from step 3, until the number of iterations reaches $iter_{max}$ or the change in the objective function J is less than a specified threshold.

3.2. The Optimal Restoration Model

The optimal coordination of ADNs, microgrids and SOPs represents a large-scale MINLP problem, requiring special methodologies to be solved efficiently. Using the linearization and conic relaxation, the supply restoration problem is defined as a mixed-integer second-order cone programming model for faster and accurate computation.

3.2.1. Objective Functions

Given the SOPs' capability to participate in the reactive power compensation, a weighted multi-objective function F is formulated in this paper, composed of three sub-objectives: supply restoration maximization, total power losses and voltage deviation minimization:

$$\min F = \alpha_1 \cdot F_{SR} + \alpha_2 \cdot F_{Losses} + \alpha_3 \cdot F_{VD} \tag{4}$$

$$F_{SR} = \sum_{t \in T} \sum_{j \in N_B} (1 - \sigma_{j,t}) \cdot w_j \cdot P_{j,t}^{D}$$

$$F_{Losses} = \sum_{t \in T} \left(\sum_{ij \in N_L} \left(R_{ij} \cdot I_{ij,t}^{sq} \right) + \sum_{i \in SOP} \left(P_{i,t}^{L,SOP} + P_{t}^{L,DC} \right) \right)$$

$$F_{VD} = \sum_{t \in T} \sum_{j \in N_B} \left| V_{j,ref} - V_{j,t} \right|$$

where α_1, α_2 and α_3 are the weight coefficients for the considered objectives. The first function, F_{SR}, models the total restored load. In this regard, the binary variable $\sigma_{j,t}$ is used for defining the supply status of load connected at bus j during time interval t (supplied or unsupplied). As the restoration capacity may be limited, a supply priority coefficient, w_j, is associated with each load, characterized by the active power demand $P_{j,t}^{D}$. The second objective considered in the study regards the total active power losses, computed using function F_{Losses}. The total power losses include the branch power losses due to the resistance R_{ij} and square value of the current $I_{ij,t}$ flowing through the line connecting buses i and j, to which the losses in the SOPs' converters, $P_{i}^{L,SOP}$, are added. Additionally, the active power losses of the DC/DC converter connecting the microgrid ($P_{t}^{L,DC}$) are considered. The third objective emphasizes the SOP's benefits in terms of voltage regulation, as it models the bus voltage ($V_{j,t}$) deviation from the reference value ($V_{j,ref}$ = 1 p.u.). Quadratic equations in the model are transformed into linear equations by variable substitution, using the square values of voltage $V_{j,t}^{sq}$ and current $I_{ij,t}^{sq}$ as independent variables. In the previous equations, the following sets have been introduced to define components of the network: N_B is the set of load buses, N_L represents the set of lines, SOP denotes the set of installation buses for the SOPs' converters, while T defines the set of time intervals used to perform the analysis.

3.2.2. ADN Operational Constraints

The restoration of electricity supply service must be carried out while satisfying the operating restrictions of the distribution network. The power flow computation is performed using the DistFlow branch model equations proposed in [31]. The active and reactive power balances at each bus j during time slot t are defined by (5) and (6), while the voltage drop on each branch and the line current are computed using (7) and (8):

$$\sum_{jk \in N_L} P_{jk,t} - \sum_{ij \in N_L} (P_{ij,t} - R_{ij} I_{ij,t}^{sq}) = P_{j,t}^{DG} + P_{j,t}^{SOP} - \sigma_{j,t} P_{j,t}^{D} \tag{5}$$

$$\sum_{jk \in N_L} Q_{jk,t} - \sum_{ij \in N_L} (Q_{ij,t} - X_{ij} I_{ij,t}^{sq}) = Q_{j,t}^{DG} + Q_{j,t}^{SOP} - \sigma_{j,t} Q_{j,t}^{D} \tag{6}$$

$$(V_{i,t}^{sq} - V_{j,t}^{sq}) - 2\left(R_{ij} P_{ij,t} + X_{ij} Q_{ij,t}\right) + (R_{ij}^2 + X_{ij}^2) \cdot I_{ij,t}^{sq} = 0 \tag{7}$$

$$I_{ij,t}^{sq} \cdot V_{i,t}^{sq} = P_{ij,t}^2 + Q_{ij,t}^2 \quad \forall ij \in N_L \tag{8}$$

Here, $P_{ij,t}$ and $Q_{ij,t}$, ($P_{jk,t}$ and $Q_{jk,t}$, respectively), denote the active and reactive power flows on the branch connecting buses i and j (j and k, respectively), during time interval t. $P^{DG}_{j,t}$ and $Q^{DG}_{j,t}$ are the active and reactive power output of the distributed generation unit installed at bus j during time interval t, while $V^{sq}_{i,t}$ and $V^{sq}_{j,t}$ represent the square of the voltage at buses i and j. The line ij parameters, resistance and reactance, are denoted by R_{ij} and X_{ij}, while $P^{D}_{j,t}$ and $Q^{D}_{j,t}$ are bus power demands.

The nonlinear terms of Equation (8) are further convex relaxed [32] and written in the second-order cone as follows:

$$\left\| \begin{matrix} 2P_{ij,t} \\ 2Q_{ij,t} \\ I^{sq}_{ij,t} - V^{sq}_{ij,t} \end{matrix} \right\|_2 \leq I^{sq}_{ij,t} + V^{sq}_{ij,t} \tag{9}$$

Equations (10) and (11) limit the DGs' output based on the operational capacity and reactive power boundaries. Here, DG defines the set of buses where renewable DGs units are connected.

$$\left(P^{DG}_{j,t}\right)^2 + \left(Q^{DG}_{j,t}\right)^2 \leq \left(S^{DG}_{j}\right)^2 \quad \forall j \in DG \tag{10}$$

$$Q^{DG}_{j,\min} \leq Q^{DG}_{j,t} \leq Q^{DG}_{j,\max} \quad \forall j \in DG \tag{11}$$

For the proper operation of the network, the following constraints regarding nodal voltage magnitudes and lines thermal limits have been defined:

$$V^2_{j,\min} \leq V^2_{j,t} \leq V^2_{j,\max} \quad \forall j \in N_B \tag{12}$$

$$0 \leq I^2_{ij,t} \leq I^2_{ij,\max} \quad \forall ij \in N_L \tag{13}$$

The radial configuration of the ADN is desired, therefore the topology constraints [33] are introduced in the model:

$$\beta_{ij} + \beta_{ji} = \lambda_{ij} \quad \forall ij \in N_L \tag{14}$$

$$\beta_{ij} = 0 \quad \forall ij \in N_L,\ i \in S \tag{15}$$

$$\sum_{ij \in N_L} \beta_{ij} = 1 \quad \forall i \notin S \tag{16}$$

where the binary variable β_{ij} is equal to 1 when j is the parent of bus i, otherwise 0. According to (15) and (16), all buses must have one parent except for the slack buses, denoted by the set S. The new network topology is established immediately after the fault occurrence that caused the power interruption and it is kept the same for the rest of the timeframes. Based on the buses parent–child correlation, the status of the line (connected/disconnected) represented by the binary variable λ_{ij} is obtained in (14).

In order to compute the voltage drop based on the status of the line connecting buses i and j, Equation (7) is replaced by (17) and (18), where M is a high-value constant. The power flowing through disconnected lines is limited to 0, based on (19) and (20):

$$(V^{sq}_{i,t} - V^{sq}_{j,t}) - 2\left(R_{ij}P_{ij,t} + X_{ij}Q_{ij,t}\right) + (R^2_{ij} + X^2_{ij}) \cdot I^{sq}_{ij,t} \geq -M(1-\lambda_{ij}) \tag{17}$$

$$(V^{sq}_{i,t} - V^{sq}_{j,t}) - 2\left(R_{ij}P_{ij,t} + X_{ij}Q_{ij,t}\right) + (R^2_{ij} + X^2_{ij}) \cdot I^{sq}_{ij,t} \leq M(1-\lambda_{ij}) \tag{18}$$

$$-M\lambda_{ij} \leq P_{ij,t} \leq M\lambda_{ij} \tag{19}$$

$$-M\lambda_{ij} \leq Q_{ij,t} \leq M\lambda_{ij} \tag{20}$$

3.2.3. *DC*-Microgrid Operation

In this study, the *DC*-microgrids contribution in supply restoration is considered as well, through a connection to the *DC* link of the SOP using a *DC*–*DC* converter. In the following equations, k represents the *DC* connection bus for the microgrid within the SOP configuration. The components of the analyzed microgrids include a *DC* load ($P_{k,t}^{MG\_L}$), a PV generation system providing the $P_{k,t}^{MG\_PV}$ output and an energy storage system. Depending on the availability of solar energy, the microgrid may encounter a surplus or a shortage of energy in supplying the local load. In this case, exchanges occur between the microgrid and the ADN, with an injection in the network taking place in the case of excess denoted by $P_{out,k,t}^{ex}$, otherwise the *MG* absorbs energy from the network to cover the local demand through the exchanged power $P_{in,k,t}^{ex}$. The power balance at the point of common coupling of the *MG* is computed based on (21), where $P_{k,t}^{ch}$ and $P_{k,t}^{disch}$ are the hourly charging and discharging powers of the ESS. The power exchange between *MG* and the ADN is limited based on (22) and (23), where $P_{\max,k}^{MG}$ is the maximum exchange quantity allowed, while the binary variable $e_{k,t}^{MG}$ ensures the avoidance of a simultaneous injection and absorption of energy. Value 1 defines the power absorption, while value 0 denotes the power injection:

$$P_{in,k,t}^{ex} - P_{out,k,t}^{ex} = P_{k,t}^{ch} + P_{k,t}^{MG\_L} - P_{k,t}^{MG\_PV} - P_{k,t}^{disch} \tag{21}$$

$$0 \leq P_{in,k,t}^{ex} \leq e_{k,t}^{MG} \cdot P_{\max,k}^{MG} \tag{22}$$

$$0 \leq P_{out,k,t}^{ex} \leq (1 - e_{k,t}^{MG}) \cdot P_{\max,k}^{MG} \tag{23}$$

The generic model used in this study for the ESS operation is defined by Equations (24)–(27):

$$P_{k,\min}^{disch} \cdot e_{k,t}^{ESS} \leq P_{k,t}^{disch} \leq P_{k,\max}^{disch} \cdot e_{k,t}^{ESS} \tag{24}$$

$$P_{k,\min}^{ch} \cdot (1 - e_{k,t}^{ESS}) \leq P_{k,t}^{ch} \leq P_{k,\max}^{ch} \cdot (1 - e_{k,t}^{ESS}) \tag{25}$$

$$SOC_{k,t} = SOC_{k,t-1} + \left(\eta_k^{ch} \cdot P_{k,t}^{ch} - P_{k,t}^{disch} / \eta_k^{disch}\right) / EC \tag{26}$$

$$SOC_{k,\min} \leq SOC_{k,t} \leq SOC_{k,\max} \tag{27}$$

Constraints (24) and (25) impose the charging and discharging boundaries of the ESS, while the binary variable $e_{k,t}^{ESS}$ defines the operation mode of the system, to avoid simultaneous charging/discharging of the device. For each timeframe t, the state of charge (*SOC*) is computed using constraint (26) based on the *SOC* corresponding to the previous time interval ($t-1$), the power charged/discharged during the current interval (t) and the system's capacity (*EC*), while also applying the charging and discharging efficiencies, η_k^{ch} and η_k^{disch}, respectively. A maximum charging capacity is defined by constraint (27), while a discharge limitation is considered as well:

$$SOC_{t1} = \alpha_{ESS} \cdot SOC_{\max} = SOC_{t24} \tag{28}$$

$$e_{k,t-1}^{ESS} - e_{k,t}^{ESS} \leq f_{k,t}^{ESS} \tag{29}$$

$$\sum_{t \in T} f_{k,t}^{ESS} \leq F_k^{ESS} \tag{30}$$

The states of charge for the first time interval of the day and for the last interval are equal and fixed based on a predefined coefficient, α_{ESS}. In order to prolong the lifespan of the device, a limitation for the number of charging/discharging cycles is imposed by constraints (29) and (30), where variable $f_{k,t}^{ESS}$ defines switches in the operation mode (from charging to discharging and vice versa), while F_k^{ESS} is the maximum admissible number of switches.

3.2.4. SOP Operational Constraints

As presented in Section 2, the SOP operation principle relies on fully controlled power electronic devices. Thus, the SOP modelling comprises as its decision variables the active and reactive powers injected by the two VSCs in the connection buses i and j ($P_{i,t}^{SOP}$, $P_{j,t}^{SOP}$, $Q_{i,t}^{SOP}$ and $Q_{j,t}^{SOP}$) and can be defined by Equations (31)–(38) [34]. In modelling the SOP operation, the DC-microgrid exchange with the network is considered as well.

(1) SOP active power constraints:

$$P_{i,t}^{SOP} + P_{j,t}^{SOP} + P_{i,t}^{L,SOP} + P_{j,t}^{L,SOP} + P_{k,t}^{L,DC} = P_{out,k,t}^{ex} - P_{in,k,t}^{ex} \tag{31}$$

$$P_{i,t}^{L,SOP} = A_i^{SOP}\sqrt{\left(P_{i,t}^{SOP}\right)^2 + \left(Q_{i,t}^{SOP}\right)^2} \tag{32}$$

$$P_{j,t}^{L,SOP} = A_j^{SOP}\sqrt{\left(P_{j,t}^{SOP}\right)^2 + \left(Q_{j,t}^{SOP}\right)^2} \tag{33}$$

$$P_{k,t}^{L,DC} = A_k^{DC}\left(P_{in,k,t}^{ex} + P_{out,k,t}^{ex}\right) \tag{34}$$

As depicted in Figure 3, the SOP-microgrid system has the following configuration: the AC sides of the SOP are connected to the ADN's feeders, while the DC sides of the two VSCs are linked with a DC–DC converter that allows the DC-microgrid installation. Based on this configuration, the active power balance of the SOP is defined by (31). Equations (32) and (33) model the active power losses occurring during the SOP's operation, where A_i^{SOP} and A_j^{SOP} are the converter's loss coefficients, while the DC–DC power losses are given in (34) based on loss coefficient A_k^{DC} and the microgrid's power exchange.

(2) SOP reactive power constraints:

$$Q_{i,\min}^{SOP} \le Q_{i,t}^{SOP} \le Q_{i,\max}^{SOP} \tag{35}$$

$$Q_{j,\min}^{SOP} \le Q_{j,t}^{SOP} \le Q_{j,\max}^{SOP} \tag{36}$$

For each VSC, reactive power output boundaries are established based on a minimum and maximum value ($Q_{j,\min}^{SOP}$ and $Q_{j,\max}^{SOP}$).

(3) SOP capacity constraints:

$$\left(P_{i,t}^{SOP}\right)^2 + \left(Q_{i,t}^{SOP}\right)^2 \le \left(S_i^{SOP}\right)^2 \tag{37}$$

$$\left(P_{j,t}^{SOP}\right)^2 + \left(Q_{j,t}^{SOP}\right)^2 \le \left(S_j^{SOP}\right)^2 \tag{38}$$

The SOP convertors' capacity is given by the maximum apparent power at each converter, S_i^{SOP} and S_j^{SOP}. As stated in [35], convex optimization techniques, such as SOCP and semidefinite programming (SDP), are widely used in studies related to SOP modelling as the P-Q operating region for back-to-back VSC topologies can be defined as a circle, which is convex. Therefore, (37) and (38) are reformulated into the following rotated quadratic constraints, with methodology also applied for the DG operation constraints:

$$\left(P_{i,t}^{SOP}\right)^2 + \left(Q_{i,t}^{SOP}\right)^2 \le 2\left(\frac{S_i^{SOP}}{\sqrt{2}}\right)\left(\frac{S_i^{SOP}}{\sqrt{2}}\right) \tag{39}$$

$$\left(P_{j,t}^{SOP}\right)^2 + \left(Q_{j,t}^{SOP}\right)^2 \le 2\left(\frac{S_j^{SOP}}{\sqrt{2}}\right)\left(\frac{S_j^{SOP}}{\sqrt{2}}\right) \tag{40}$$

4. Case Study

4.1. The Modified IEEE 33−Bus System

In this section, the SOP-microgrid restoration methodology is analyzed and verified using a modified IEEE 33−bus active distribution network. The detailed parameters regarding the maximum bus loads and the lines are specified in [36]. The network's voltage level was 12.66 kV, while the lower and upper bounds of bus voltages were set to 0.95 p.u. and 1.05 p.u., respectively. Six DG units, including two wind turbines and four PVs, were installed in the system. The wind turbine capacity was 450 kVA, while the PV's capacity was 200 kVA. For both generation technologies, the power factor was set from 0.9 lagging to 0.9 leading. Three user types (i.e., residential, commercial and industrial) were randomly associated to the buses, as depicted in Figure 4. Considering a limited capability of restoration, a priority coefficient was assigned to each load, as presented in Table 1. Two SOP devices were installed in the network, between buses 12 and 22, and between buses 18 and 33, respectively. The parameters for the two SOPs are presented in Table 2, with values of the converter losses coefficients of 2% [37]. The *DC*-microgrids' configuration considered in the study consisted of a *DC* load, a PV generation unit and an energy storage system (ESS), of which the parameters are introduced in Table 3.

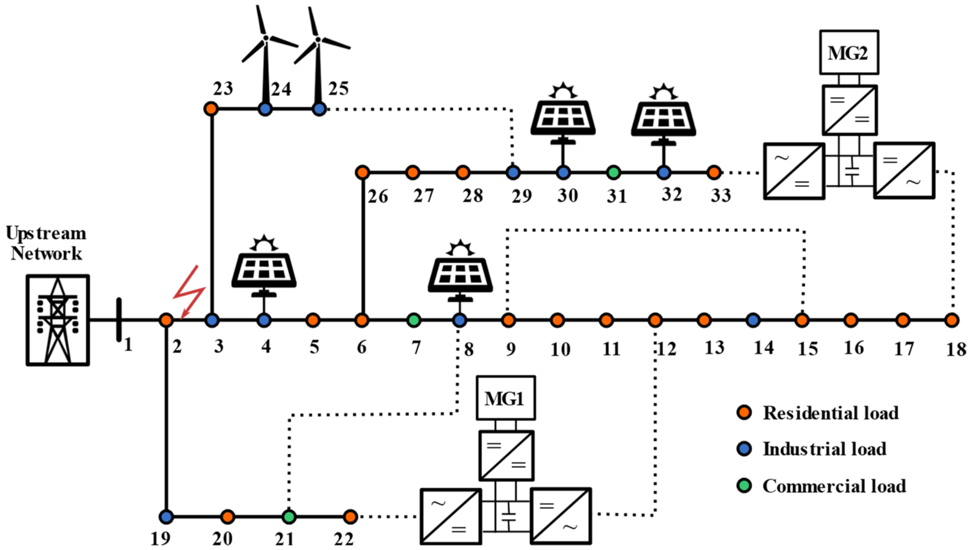

Figure 4. The modified IEEE 33−bus system.

Table 1. Priority weight coefficient of load.

Priority Category	w_j	Node of Load
I	10	8, 11, 14, 21, 24, 30,
II	5	7, 10, 19, 25, 27, 29, 32
III	1	2, 3, 4, 5, 6, 9, 12, 13, 15, 16, 17, 18, 20, 22, 23, 26, 28, 31, 33

Table 2. Basic installation parameters of the SOP.

SOP Placement	Maximum Capacity	Reactive Power Limits	Active Power Losses
12–22	1000 kVA	[−600, 600] kvar	2%
18–33	1000 kVA	[−600, 600] kvar	2%

Table 3. Basic parameters for the *DC*-microgrids components.

Component	Parameter	Value
Load	$P_{\max}^{MG\_L}$	150 kW
	Type	$MG1$–Commercial $MG2$–Industrial
PV	$P_{\max}^{MG\_PV}$	450 kWp
	Power factor ($cos\varphi$)	1
ESS	EC	1000 kWh
	$SOC_{\min}$	0.2
	$SOC_{\max}$	0.98
	$P_{\min}^{ch}$	0
	$P_{\max}^{ch}$	0.2
	$P_{\min}^{disch}$	0
	$P_{\max}^{disch}$	0.35
	η^{ch}	0.9
	η^{disch}	0.85
	α_{ESS}	0.4
	F^{ESS}	2
DC–DC converter	A^{DC}	1%
	$P_{\max}^{MG}$	200 kW

The analysis further conducted in this study involved the 24-h scheduling of the ADN's elements, thus load and generation profiles were required. As previously mentioned, electrical loads can be divided into three categories, namely, residential, commercial and industrial [38,39]. Residential consumption data were collected from the OpenEI platform [40], while the commercial and industrial profiles comprised hourly measurements from corresponding entities located in Bucharest, Romania. Wind and photovoltaic generation profiles were obtained using the Renewables.ninja simulation tool [41]. The load and generation data consisted of hourly normalized values for a one year period.

The uncertainties computation was performed in MATLAB R2020a, while the optimization model was solved by GAMS 24.0.2, using CPLEX solver, on a PC with Intel Core i5-9500F 3.00 GHz CPU and 16 GB RAM.

4.2. Load and Generation Uncertainties Modelling Results Based on FCM Clustering Technique

In this paper, the uncertainties regarding load and generation are handled by employing the FCM clustering algorithm to identify the most representative scenarios derived from the considered dataset and to further apply the optimization model using the formed clusters centers. In this study, each scenario was defined by the 24-h profiles for loads (residential, commercial and industrial) and generation (PV and wind).

Given that the FCM algorithm belongs in the unsupervised learning paradigm, the optimal number and partition of clusters is unknown, as the algorithm has no defined target. Therefore, a crucial task in clustering analysis consists of selecting the proper number of clusters. In this regard, cluster validation indices (CVIs) are defined to quantitatively evaluate the validity of the clustering results. CVIs usually assess two features of clusters, namely, the compactness, which measures the similarity between data in the same cluster, and separation, which measures the diversity of clusters [42]. Several CVIs were proposed in the literature, such as the partition coefficient (PC), the modified partition coefficient (MPC), the partition entropy (PE) and the Xie–Beni coefficient (XB) [43], described by the following equations:

$$PC = \frac{1}{N}\sum_{i=1}^{N}\sum_{j=1}^{C}\mu_{ij}^{m} \tag{41}$$

$$MPC = 1 - \frac{C}{C-1}(1 - \sum_{i=1}^{N}\sum_{j=1}^{C}\mu_{ij}^{2}) \tag{42}$$

$$PE = -\frac{1}{N}\sum_{i=1}^{N}\sum_{j=1}^{C}\mu_{ij}\log(\mu_{ij}) \tag{43}$$

$$XB = \frac{\sum_{i=1}^{N}\sum_{j=1}^{C}\mu_{ij}^{m}\|x_i - c_j\|^2}{N(\min\{c_i - c_k\})} \tag{44}$$

In the previous equations, higher values of PC and MPC coefficients indicate a better cluster partition. On the other hand, the best number of clusters is attained at the lowest values of PE and XB. Results from different CVIs may not indicate the same number of clusters as being optimal, thus it was necessary to conduct an analysis based on multiple evaluation metrics and to choose the most suited number of clusters. Considering the optimal number of clusters contained in the $\left[2, \sqrt{N}\right]$ range [44], the FCM algorithm was carried out for the 365 days dataset, modifying the number of clusters from 2 to 20. Figure 5 depicts the previously mentioned CVIs values that resulted from each simulation.

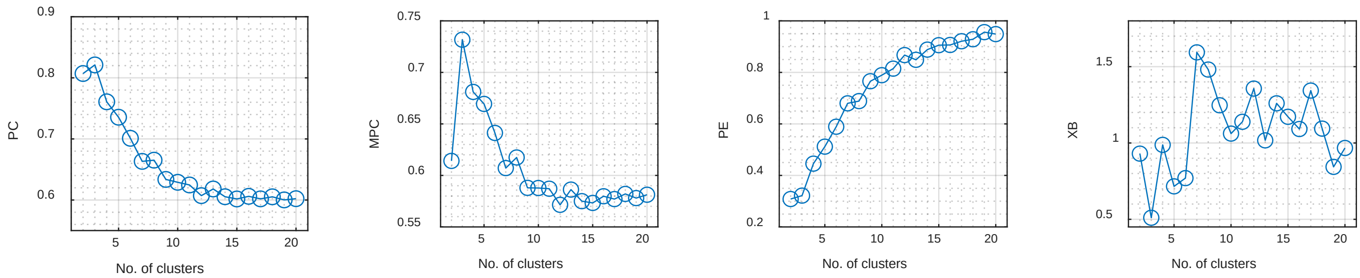

(**a**) (**b**) (**c**) (**d**)

Figure 5. Comparison of cluster validation indices for various number of clusters: (**a**) partition coefficient; (**b**) modified partition coefficient; (**c**) partition entropy; and (**d**) Xie–Beni coefficient.

As depicted in Figure 5, the maximum values for PC and MPC were obtained when the number of clusters was set to three. Likewise, the XB coefficient achieved its minimum value with three clusters. Despite the PE coefficient's lowest value being obtained for two clusters, the simulation with three clusters resulted in a close value of the PE (i.e., 0.308 for two clusters and 0.322 for three clusters). Therefore, it can be concluded that three clusters were optimal for extracting the most representative scenarios from the studied dataset. Figure 6 depicts the three obtained cluster centers, which represent the scenarios further employed in the study.

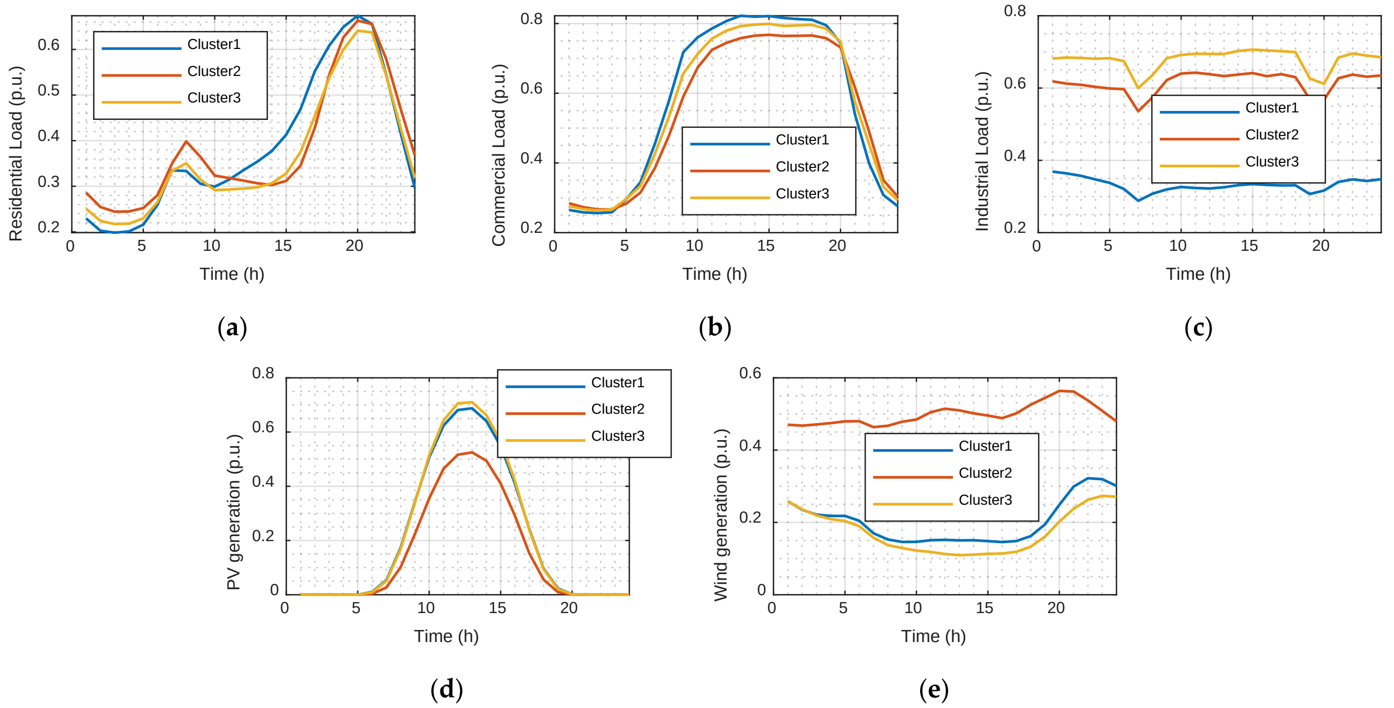

Figure 6. Cluster centers for the load and generation scenarios: (**a**) residential load; (**b**) commercial load; (**c**) industrial load; (**d**) PV generation; and (**e**) wind generation.

5. Discussion on Restoration Results

In order to validate the effectiveness of the SOP-microgrid coordination model proposed in this paper, two schemes were investigated for comparative analysis, including a supply restoration strategy based on reconfiguration and tie switches (Scheme I), and the proposed supply restoration methodology based on reconfiguration and SOP with embedded *DC*-microgrids (Scheme II). Assuming a permanent three-phase fault occurring on line 2–3 during the first hour of the day, a blackout area downstream of node three was formed. At the same time, all the distributed generation units in the affected area were disconnected, resulting in a total unsupplied load of 87.51%. Based on these premises, the two restoration schemes were applied to resume the power supply service of the blackout area. The reconfiguration process is the generally applied restoration strategy [44], which is based on connecting and disconnecting branches in the network, to obtain a new supply topology; however, since the tie switches did not provide voltage support, the restoration ratio was reduced to maintain the voltage within specified limits for the re-energized load. This restoration scheme served as a benchmark for the proposed restoration strategy, as the SOPs voltage regulation capabilities was investigated.

Firstly, a detailed analysis was performed using the first cluster center for the load and generation scenarios, followed by an overall analysis for all the clusters. The three weight coefficients in the objective function (α_1, α_2 and α_3) were considered 0.7, 0.15 and 0.15, respectively.

5.1. Scheme I Restoration Results

The base configuration of IEEE 33-bus system contained 32 sectionalized lines and 5 normally-opened tie switches, installed on branches 8–12, 9–15, 12–22, 18–33 and 25–29, respectively. As previously mentioned, the first restoration scheme applied in the study was based solely on the reconfiguration process, considering the maximum capacity for NOPs of 1000 kVA. Figure 7 illustrates the new ADN topology applied for maximizing the re-energized load. As can be observed, a radial configuration resulted by connecting lines 8–21, 12–22, 25–29 and 18–33, while 4–5, 8–9, 9–15, and 29–30 were disconnected, additional to the faulted line 2–3.

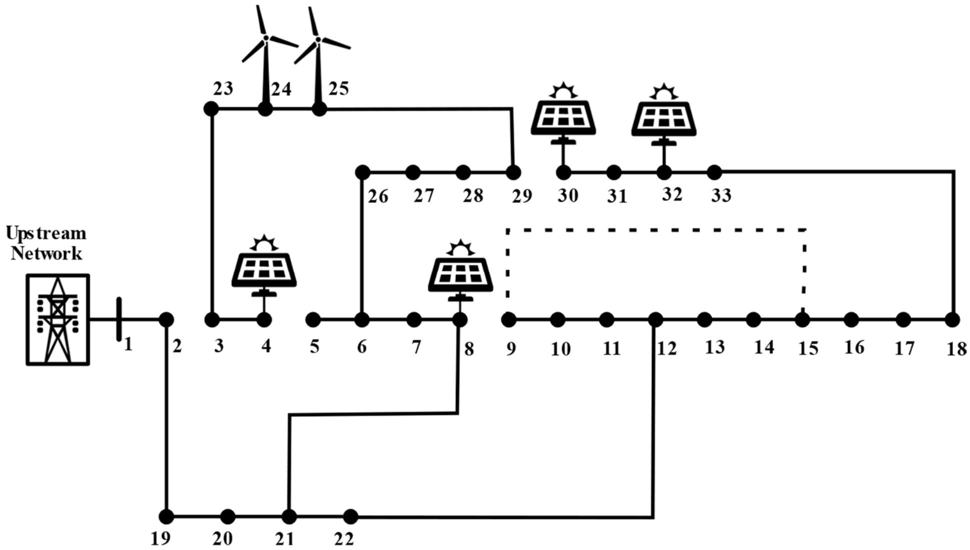

Figure 7. Restoration results for Scheme I.

The restoration rate for each type of load, based on their priority ranking, is presented in Figure 8. During the first hours of the day, the distribution grid was able to fully restore the supply on both the first and second priority loads, as well as assuring a degree of restoration rate for the third priority loads of more than 60%. As the distribution grid's voltage constraints must be satisfied, a reduction of the restored supply for non-critical loads can be observed during peak load periods (i.e., 06.00–09.00 and 16.00–23.00). The PV generation units contributed significantly to increasing the supply rate in the 09.00–17.00 interval, especially for the second priority degree loads. The overall restoration rates for the first, second and third priority loads, respectively, were 99.65%, 70.69% and 32.81%.

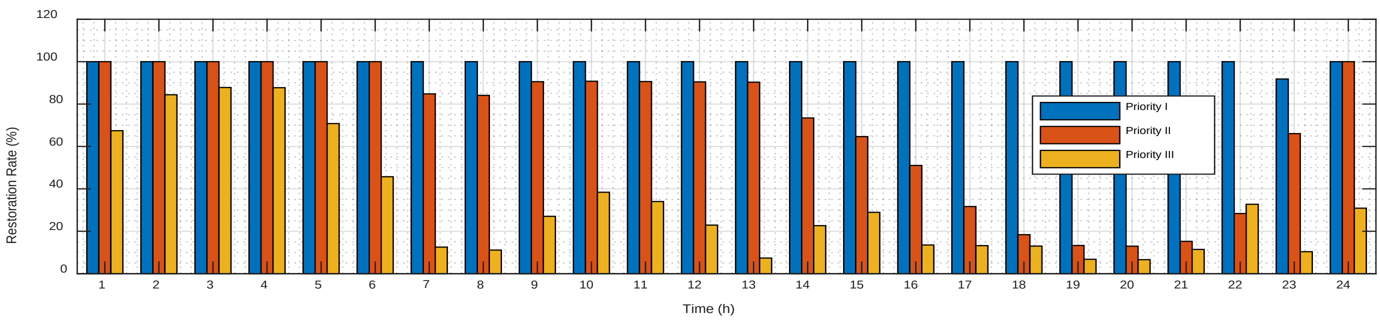

Figure 8. Restoration ratios for Scheme I.

Figure 9 depicts the boxplot representations of bus voltages and the average voltage for each hour of the analysis, while Figure 10 illustrates the minimum and maximum voltage of each bus over the day. The best voltage profile occurred at 13.00, as the PV production reached its maximum value. Despite the voltage being maintained above the imposed limit of 0.95 p.u. throughout the day, it can be observed that the average voltage value was confined in the [0.96, 0.97] p.u. range, as the voltage regulation capability of the network was insufficient to assure a better voltage profile; however, the boxplots depict several outliers, which represent buses with higher voltages, achieving values close to 1 p.u. By analyzing Figure 10 it can be determined that the aforementioned buses were 1, 2 and 19, respectively. Bus 1 represents the slack bus, while 2 and 19 are its neighboring buses, thus, their voltages remained close to the rated value. During several hours of the day (e.g., 10th, 11th, 15th, and 18th) the voltage level decreased as a result of the higher demand. The influence of DG reactive power compensation is highlighted in Figure 10, as the connection buses 8, 30 and 32 displayed a better voltage level compared to adjacent buses.

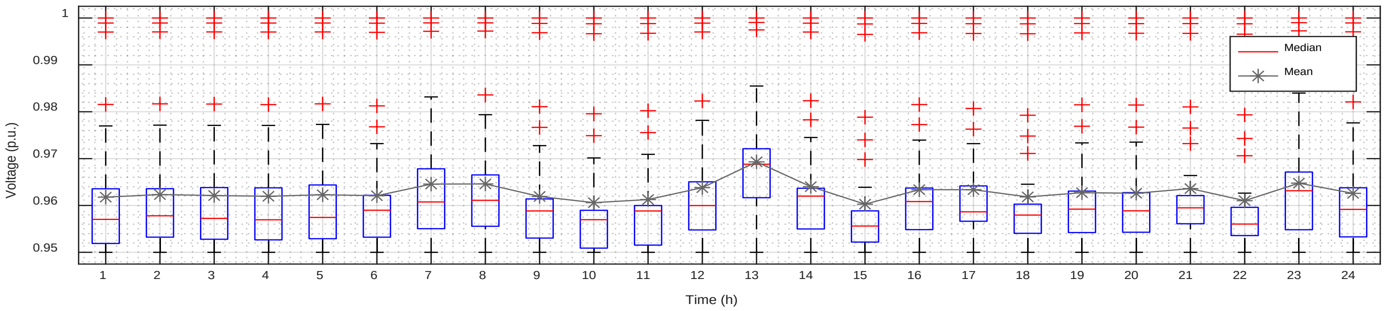

Figure 9. Boxplot representation of hourly voltage profiles for Scheme I.

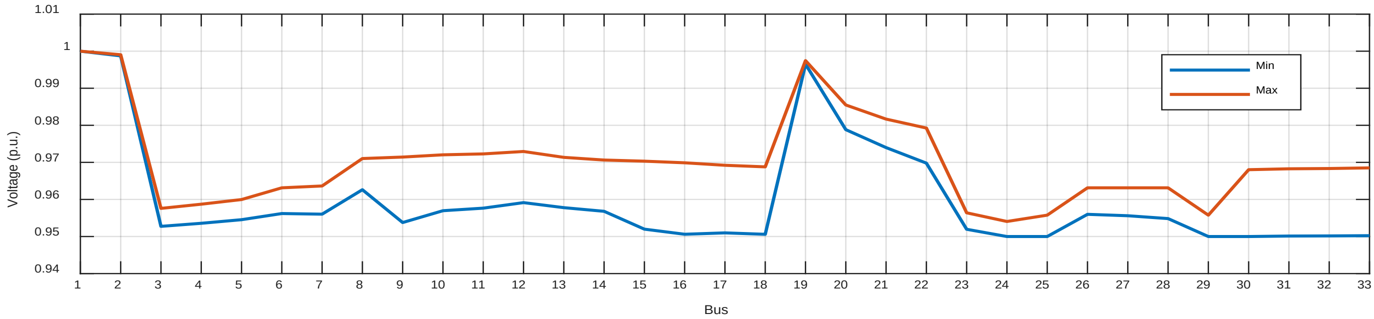

Figure 10. Minimum and maximum bus voltages for Scheme I.

5.2. Scheme II Restoration Results

For the second restoration scheme, the tie switches connecting buses 18–33 and 12–22 were replaced by two SOPs, which incorporated the considered *DC*-microgrids. The new grid topology was obtained after the reconfiguration process, connecting lines 8–21 and 9–15 and disconnecting lines 6–26, 9–10, 14–15 and 25–29, as depicted in Figure 11.

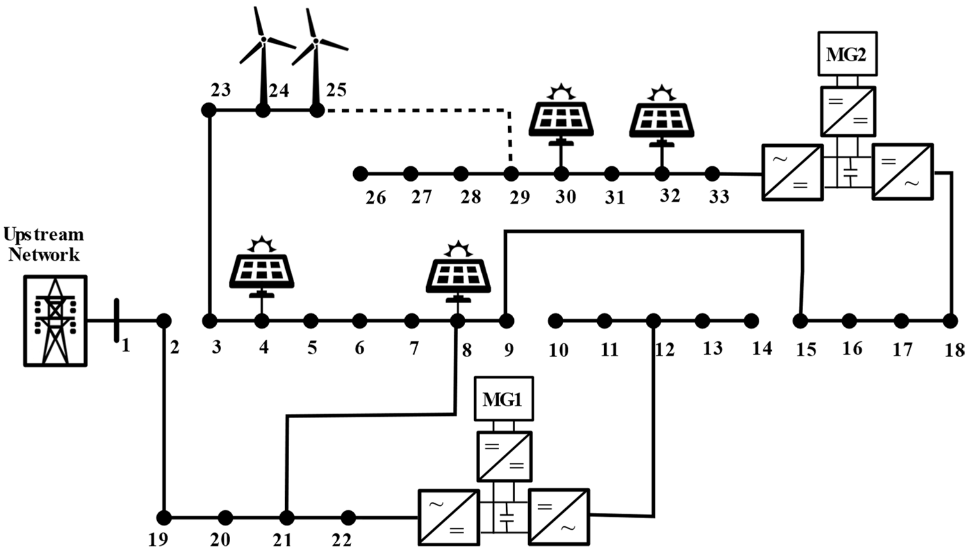

Figure 11. Restoration results for Scheme II.

The two *DC*-microgrids operation scheduling is depicted in Figure 12. The energy production in the microgrid is illustrated as positive values, including the PV generation, the ESS discharging and the power absorption from the ADN, while the energy consumption is represented as negative values (demand, ESS charging and the injection in the ADN). It can be observed that the charging of the ESS took place during the day, when the PV production was high, while the discharging occurred during the demand peaks (08.00–09.00 and 18.00–21.00). A collaboration scheme can be observed between the ADN and the microgrids, with the latter absorbing energy from the network during the off-peak hours to supply the local load, while the PV production surplus obtained during the day was used to charge the storage system or was injected into the distribution network. A higher injection in the ADN can be observed for the second microgrid compared to the first microgrid, as the industrial consumption was lower for the analyzed cluster. Figure 13 shows the SOPs' outputs in terms of active and reactive power. The discrepancies in values for the active power injected by the two converters of the SOPs are due to power losses and the injection/absorption of energy from the microgrids. It can be observed that during the whole day, the active power flowed from bus 22 to bus 12 and from bus 33 to bus 18, respectively. Considering the low voltage level that resulted in the first restoration scheme, the ADN required reactive power sources to improve the voltage. Consequently, the SOP converters at buses 18 and 22 were operating at their maximum capacity for most of the analyzed day. Increased values can be observed for converters 12 and 33 during the peak load hours (16.00–23.00), aimed at a voltage profile improvement.

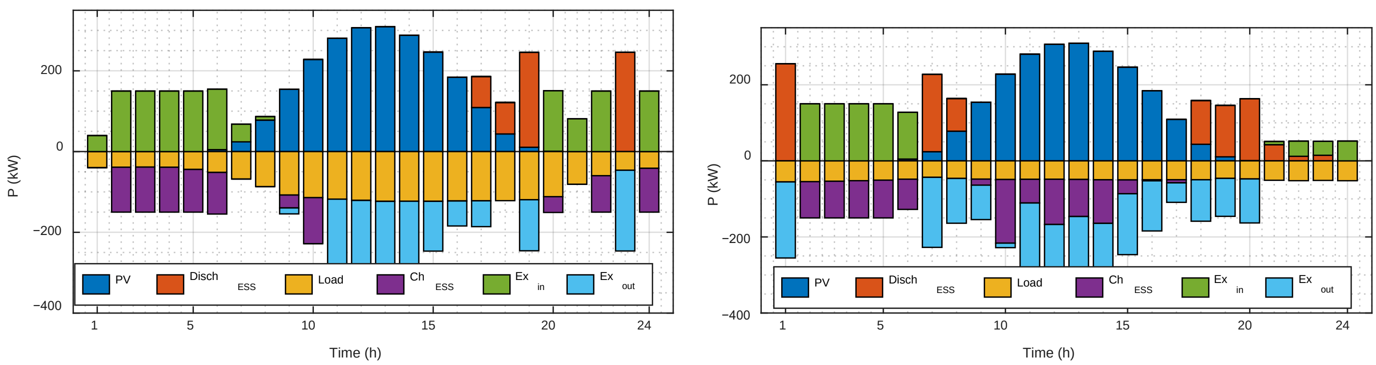

(**a**) (**b**)

Figure 12. *DC*-microgrids scheduling for: (**a**) *MG*1; and (**b**) *MG*2.

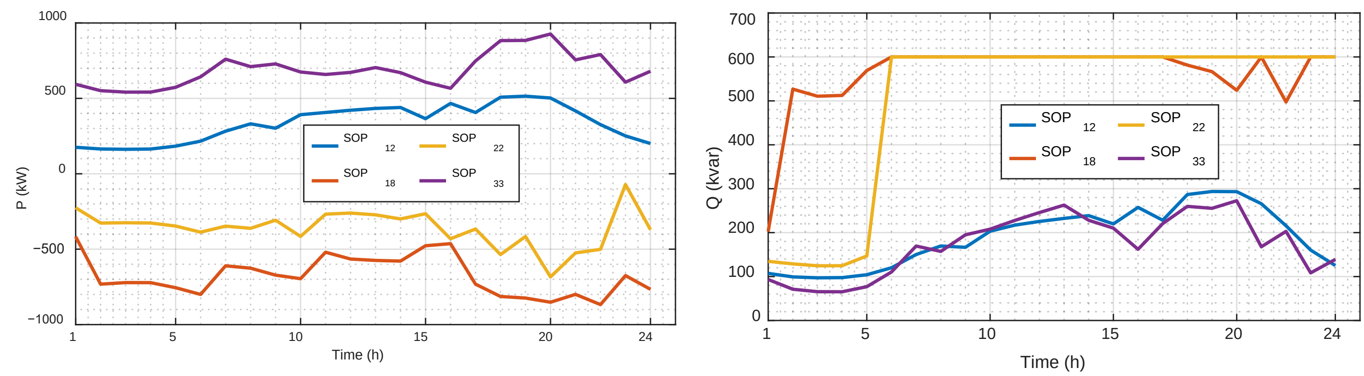

(**a**) (**b**)

Figure 13. SOPs' converters output: (**a**) active power; and (**b**) reactive power.

To further analyze the influence of the SOP on the supply recovery, the restoration rates for the three classes of loads are shown in Figure 14. A substantial improvement can be observed for this restoration scheme, as the first priority loads were completely supplied for the entire day. The SOP's generation of reactive power reduced the line loadings, expanding the active power flow capacity in the ADN. As a result, the obtained restoration ratios for priorities I, II and III loads were as follows: 100%, 87.55% and 60.94%, respectively.

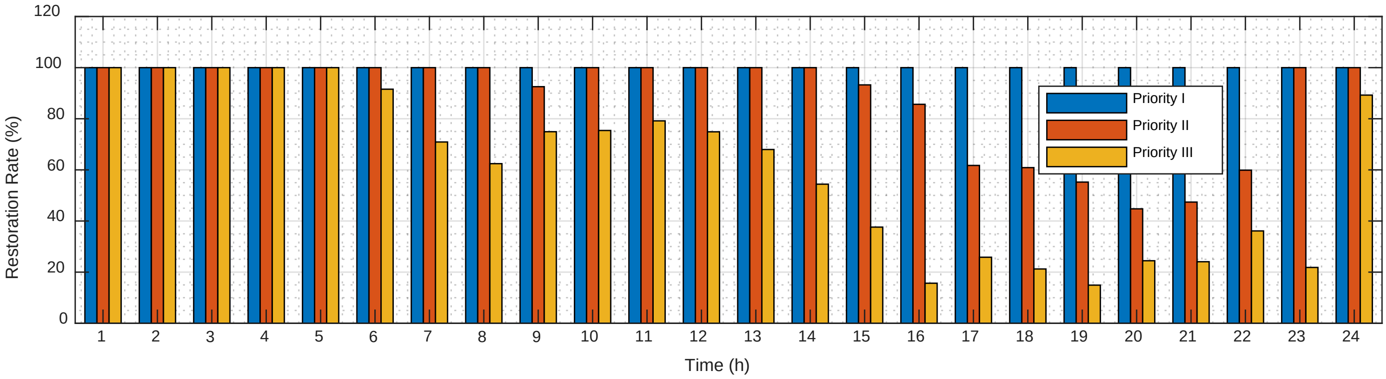

Figure 14. Restoration ratios for Scheme II.

The SOP's voltage support capability can be observed in the bus voltage profiles illustrated in Figures 15 and 16. An improvement on the voltage profiles was achieved over the entire day, including the load peak intervals, as the average bus voltage throughout the day in the SOP restoration scheme lies in the [0.97, 0.99] p.u. range. Due to the reactive power injection of SOPs, the maximum bus voltage within the network surpassed 1 p.u. (the slack bus voltage), reaching a maximum value of 1.026 p.u., recorded for bus 33 at 17.00. The minimum and the maximum voltage recorded for each bus during the 24-h analysis are depicted in Figure 16, which better highlights the benefits of SOPs and microgrids support in ADN voltage regulation. It can be observed that the minimum and maximum voltages at the SOPs buses (i.e., 12, 18, 22 and 33) present a noticeable improvement compared to the first restoration scheme, with the SOPs maintaining the voltage at the connection bus close to 1 p.u. for the whole day (e.g., the minimum and maximum voltage for bus 12 were 1.002 p.u. and 1.014 p.u., respectively).

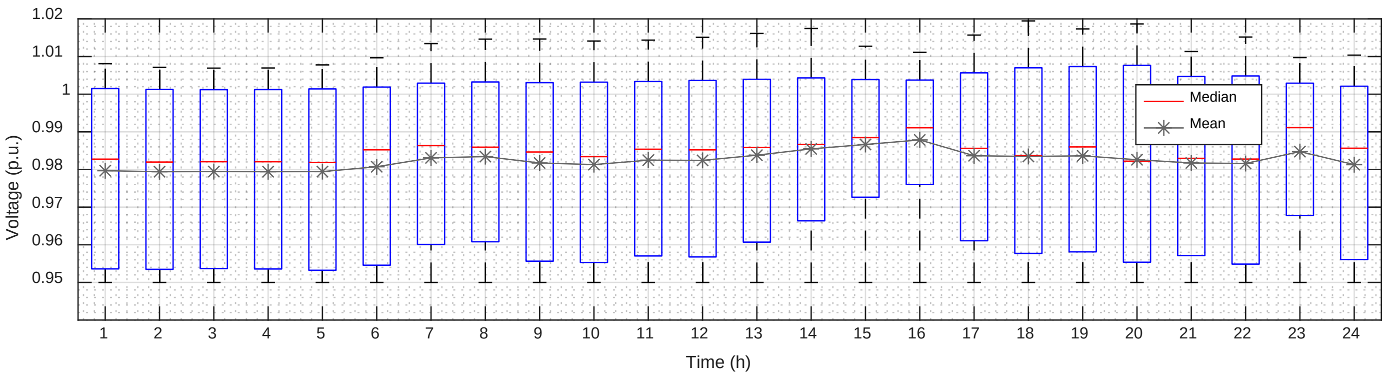

Figure 15. Boxplot representation of hourly voltage profiles for Scheme II.

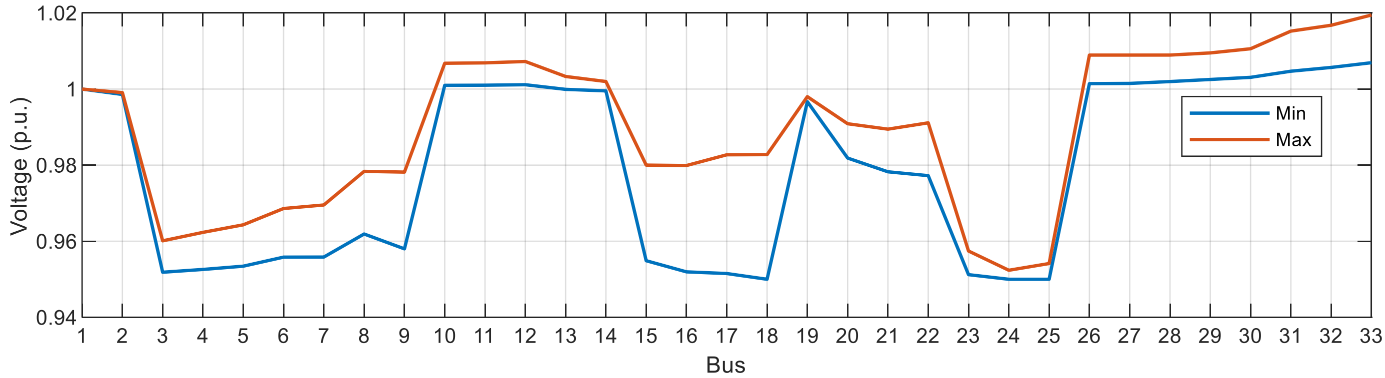

Figure 16. Minimum and maximum bus voltages in Scheme II.

5.3. Overall Results and Scheme Comparison

In this section, the two restoration schemes' performances are compared for the three clusters. The supply restoration results, as well as the total voltage deviations obtained for the two schemes are shown in Tables 4 and 5. SOPs and *DC*-microgrids integration shows a stronger supply restoration capability than a standard reconfiguration with NOPs. Comparing Schemes I and II, it can be seen that more load could be recovered in Scheme II, as the *MG*'s ESS could effectively realize the temporal power regulation by charging or discharging, while the SOPs provided advanced power flow control and voltage support leading to an increased loadability of the electrical lines by providing the local demand of reactive power. The SOP + *MG* methodology attained a 100% supply of the priority I loads for each scenario, while Scheme I failed to fully recover the critical loads. Scheme II displayed better results for the priority II and III loads as well, reaching for priority II load restoration ratios of ~85–92% for all clusters. Despite the restoration rate improvement ensured by the SOPs and *MG*s in Scheme II, the ADN load could not be totally restored, as the operational constraints (i.e., voltage limit and maximum line current) needed to be satisfied. As the cluster 2 modelled high generation from the wind turbines, an increased recovery rate could be observed for both restoration schemes; however, due to the higher demand as well, the loading on the ADN led to increased voltage drops, resulting in greater voltage deviation. On the other hand, cluster 3 implied a high consumption for industrial users simultaneously with a low wind generation, thus, the rate of restoration was reduced. Nonetheless, the overall restoration ratios of Scheme II were improved by 16–17%.

Table 4. Total load restoration rates.

	Reconfiguration			**SOP with *MG***		
	Priority I	**Priority II**	**Priority III**	**Priority I**	**Priority II**	**Priority III**
Cluster 1	99.65	70.69	32.81	100	87.55	60.94
Cluster 2	99.67	81.82	36.1	100	91.47	64.91
Cluster 3	99.3	74.08	29.53	100	84.55	57.88

Table 5. Voltage deviation results.

	Reconfiguration		**SOP with *MG***	
	Total	**Average (p.u.)**	**Total**	**Average (p.u.)**
Cluster 1	14.8651	0.0188	8.7164	0.011
Cluster 2	15.4687	0.0195	12.1674	0.0153
Cluster 3	14.8256	0.0187	11.2003	0.0141

The voltage profile enhancement represents a crucial feature in the transition to an ADN, as it leads to improvements regarding active power losses, line loadings and supply restoration capacity. Therefore, optimization models should focus on this objective as well. The total voltage deviation, computed as a sum of all bus voltage deviations from the nominal value of 1 p.u., is presented in Table 5. The performance of SOPs in voltage regulation is reflected in the results below, as the total voltage deviation was reduced by up to 41% for cluster 1, 21% for cluster 2, and 24.4% for cluster 3, using the SOP and MG support scheme, compared to the standard reconfiguration process.

6. Conclusions

The paradigm of active distribution networks relies on an integration of advanced technologies to increase the hosting capacity of distributed generation and to improve the quality of the supply. Soft open points, consisting in two back-to-back voltage source converters, represent devices that can provide high flexibility to distribution networks, controlling the active power flow through the device and regulating voltage at each connection point based on the injection or absorption of reactive power. Another emerging trend is the implementation of microgrids, particularly *DC* microgrids, as most modern appliances are supplied in *DC*. Resilience becomes a crucial feature of active distribution networks, thus, modern solutions for service restoration in the case of outages are required in order to maintain supply continuity. This paper proposes a deterministic optimization model to solve the load supply restoration problem, considering the presence of renewable energy sources, soft open points and *DC* microgrids support, by embedding the latter on the *DC* side of SOPs. The aim of the optimization model is to maximize the supply restoration rate, considering multiple degrees of priority, while also improving the voltage profile and reducing the power losses. For the case study, the IEEE 33-bus system was chosen to highlight the performance of the soft open points and *DC* microgrids restoration strategy in comparison to the standard reconfiguration process. Load and generation uncertainties are modelled in this paper by employing the Fuzzy c-means clustering technique and generating three representative scenarios, which are further investigated. The results of the two restoration schemes showed that SOPs in conjunction with microgrids support can lead to an improvement of the total restored load by up to 17%, compared to the classical reconfiguration model. Furthermore, the benefits provided by the proposed methodology are reflected by the voltage profile enhancement, with the SOP + microgrid scheme achieving a 40% reduction of total voltage deviation from the nominal value compared to the reconfiguration scheme.

Author Contributions: Conceptualization, I.I.P.; methodology, I.I.P. and A.M.T.; software, I.I.P. and A.M.T.; validation, I.I.P., C.B.; formal analysis, I.I.P.; investigation, I.I.P., A.M.T. and D.O.S.; resources, A.M.T. and D.O.S.; data curation, I.I.P. and A.M.T.; writing—original draft preparation, I.I.P., A.M.T. and D.O.S.; writing—review and editing, A.M.T. and D.O.S.; visualization, I.I.P.; supervision, C.B.; project administration, I.I.P.; funding acquisition, C.B. All authors have read and agreed to the published version of the manuscript.

Funding: This research received no external funding.

Conflicts of Interest: The authors declare no conflict of interest.

References

1. Davarzani, S.; Pisica, I.; Taylor, G.A.; Munisami, K.J. Residential Demand Response Strategies and Applications in Active Distribution Network Management. *Renew. Sustain. Energy Rev.* **2021**, *138*, 110567. [CrossRef]
2. Long, C.; Wu, J.; Thomas, L.; Jenkins, N. Optimal operation of soft open points in medium voltage electrical distribution networks with distributed generation. *Appl. Energy* **2016**, *184*, 427–437. [CrossRef]
3. Qi, Q.; Wu, J.; Long, C. Multi-objective operation optimization of an electrical distribution network with soft open point. *Appl. Energy* **2017**, *208*, 734–744. [CrossRef]
4. Cao, W.; Wu, J.; Jenkins, N.; Wang, C.; Green, T. Benefits analysis of Soft Open Points for electrical distribution network operation. *Appl. Energy* **2016**, *165*, 36–47. [CrossRef]
5. Diaaeldin, I.; Abdel Aleem, S.; El-Rafei, A.; Abdelaziz, A.; Zobaa, A.F. Optimal Network Reconfiguration in Active Distribution Networks with Soft Open Points and Distributed Generation. *Energies* **2019**, *12*, 4172. [CrossRef]
6. Wang, C.; Song, G.; Li, P.; Ji, H.; Zhao, J.; Wu, J. Optimal siting and sizing of soft open points in active electrical distribution networks. *Appl. Energy* **2017**, *189*, 301–309. [CrossRef]
7. Xiao, H.; Pei, W.; Li, K. Optimal Sizing and Siting of Soft Open Point for Improving the Three Phase Unbalance of the Distribution Network. In Proceedings of the 21st International Conference on Electrical Machines and Systems (ICEMS), Jeju, Korea, 7–10 October 2018.
8. Justo, J.J.; Mwasilu, F.; Lee, J.; Jung, J.W. AC-microgrids versus DC-microgrids with distributed energy resources: A review. *Renew. Sustain. Energy Rev.* **2013**, *24*, 387–405. [CrossRef]
9. Lotfi, H.; Khodaei, A. AC Versus DC Microgrid Planning. *IEEE Trans. Smart Grid* **2017**, *8*, 296–304. [CrossRef]
10. Habeeb, S.A.; Tostado-Véliz, M.; Hasanien, H.M.; Turky, R.A.; Meteab, W.K.; Jurado, F. DC Nanogrids for Integration of Demand Response and Electric Vehicle Charging Infrastructures: Appraisal, Optimal Scheduling and Analysis. *Electronics* **2021**, *10*, 2484. [CrossRef]
11. Al-Ismail, F.S. DC Microgrid Planning, Operation, and Control: A Comprehensive Review. *IEEE Access* **2021**, *9*, 36154–36172. [CrossRef]
12. Iovine, A.; Rigaut, T.; Damm, G.; De Santis, E.; Di Benedetto, M.D. Power management for a DC MicroGrid integrating renewables and storages. *Control Eng. Pract.* **2019**, *85*, 59–79. [CrossRef]
13. Che, L.; Khodayar, M.; Shahidehpour, M. Only Connect: Microgrids for Distribution System Restoration. *IEEE Power Energy Mag.* **2014**, *12*, 70–81.

14. Gao, H.; Chen, Y.; Xu, Y.; Liu, C. Resilience-Oriented Critical Load Restoration Using Microgrids in Distribution Systems. *IEEE Trans. Smart Grid* **2016**, *7*, 2837–2848. [CrossRef]
15. Yao, C.; Zhou, C.; Yu, J.; Xu, K.; Li, P.; Song, G. A Sequential Optimization Method for Soft Open Point Integrated with Energy Storage in Active Distribution Networks. *Energy Procedia* **2018**, *145*, 528–533. [CrossRef]
16. Ehsan, A.; Yang, Q. State-of-the-art techniques for modelling of uncertainties in active distribution network planning: A review. *Appl. Energy* **2019**, *239*, 1509–1523. [CrossRef]
17. Refaat, M.M.; Aleem, S.H.E.A.; Atia, Y.; Ali, Z.M.; El-Shahat, A.; Sayed, M.M. A Mathematical Approach to Simultaneously Plan Generation and Transmission Expansion Based on Fault Current Limiters and Reliability Constraints. *Mathematics* **2021**, *9*, 2771. [CrossRef]
18. Neagu, B.C.; Grigoras, G. Uncertainty-Based Decision Making in the Planning of Electric Transmission Networks. In Proceedings of the 11th International Conference on Electronics, Computers and Artificial Intelligence (ECAI), Pitesti, Romania, 27–29 June 2019.
19. Bloemink, J.M.; Green, T.C. Increasing Distributed Generation Penetration Using Soft Normally-Open Points. In Proceedings of the IEEE PES General Meeting, Minneapolis, MN, USA, 25–29 July 2010.
20. Ali, Z.M.; Diaaeldin, I.M.; El-Rafei, A.; Hasanien, H.M.; Abdel Aleem, S.H.; Abdelaziz, A.Y. A novel distributed generation planning algorithm via graphically-based network reconfiguration and soft open points placement using Archimedes optimization algorithm. *Ain Shams Eng. J.* **2021**, *12*, 1923–1941. [CrossRef]
21. Bai, L.; Jiang, T.; Li, F.; Chen, H.; Li, X. Distributed energy storage planning in soft open point based active distribution networks incorporating network reconfiguration and DG reactive power capability. *Appl. Energy* **2018**, *210*, 1082–1091. [CrossRef]
22. Mudaliyar, S.; Mishra, S. Real-Time Coordinated Control of Low-Voltage DC Distribution Network with Soft Opening Point. *IEEE Trans. Power Electron.* **2021**, *36*, 7123–7137. [CrossRef]
23. Abdelrahman, M.A.; Long, C.; Wu, J.; Jenkins, N. Optimal Operation of Multi-Terminal Soft Open Point to Increase Hosting Capacity of Distributed Generation in Medium Voltage Networks. In Proceedings of the 2018 53rd International Universities Power Engineering Conference (UPEC), Glasgow, UK, 4–7 September 2018.
24. Aithal, A.; Long, C.; Cao, W.; Wu, J.; Ugalde-Loo, C.E. Impact of soft open point on feeder automation. In Proceedings of the 2016 IEEE International Energy Conference (ENERGYCON), Leuven, Belgium, 4–8 April 2016.
25. Cao, W.; Wu, J.; Jenkins, N.; Wang, C.; Green, T. Operating Principle of Soft Open Points for Electrical Distribution Network Operation. *Appl. Energy* **2016**, *164*, 245–257. [CrossRef]
26. Xiang, Y.; Liu, J.; Li, F.; Liu, Y.; Liu, Y.; Xu, R.; Su, Y.; Ding, L. Optimal Active Distribution Network Planning: A Review. *Electr. Power Compon. Syst.* **2016**, *44*, 1075–1094. [CrossRef]
27. Fathabadi, H. Power distribution network reconfiguration for power loss minimization using novel dynamic fuzzy c-means (dFCM) clustering based ANN approach. *Int. J. Electr. Power Energy Syst.* **2016**, *78*, 96–107. [CrossRef]
28. Yan, R.; Wang, J.; Lu, S.; Ma, Z.; Zhou, Y.; Zhang, L.; Cheng, Y. Multi-objective two-stage adaptive robust planning method for an integrated energy system considering load uncertainty. *Energy Build.* **2021**, *235*, 110741. [CrossRef]
29. Benmouiza, K.; Tadj, M.; Cheknane, A. Classification of hourly solar radiation using fuzzy c-means algorithm for optimal stand-alone PV system sizing. *IEEE Syst. J.* **2016**, *82*, 233–241. [CrossRef]
30. Baran, M.E.; Wu, F.F. Network reconfiguration in distribution systems for loss reduction and load balancing. *IEEE Trans. Power Deliv.* **1989**, *4*, 1401–1407. [CrossRef]
31. Li, Y.; Xiao, J.; Chen, C.; Tan, Y.; Cao, Y. Service Restoration Model with Mixed-Integer Second-Order Cone Programming for Distribution Network with Distributed Generations. *IEEE Trans. Smart Grid* **2019**, *10*, 4138–4150. [CrossRef]
32. Lee, C.; Liu, C.; Mehrotra, S.; Bie, Z. Robust Distribution Network Reconfiguration. *IEEE Trans. Smart Grid* **2015**, *6*, 836–842. [CrossRef]
33. Li, P.; Ji, H.; Wang, C.; Zhao, J.; Song, G.; Ding, F.; Wu, J. Coordinated Control Method of Voltage and Reactive Power for Active Distribution Networks Based on Soft Open Point. *IEEE Trans. Sustain. Energy* **2017**, *8*, 1430–1442. [CrossRef]
34. Lou, C.; Yang, J.; Li, T.; Vega-Fuentes, E. New phase-changing soft open point and impacts on optimising unbalanced power distribution networks. *IET Gener. Transm. Distrib.* **2020**, *14*, 5685–5696. [CrossRef]
35. Wan, C.; Lin, J.; Guo, W.; Song, Y. Maximum Uncertainty Boundary of Volatile Distributed Generation in Active Distribution Network. *IEEE Trans. Smart Grid* **2018**, *9*, 2930–2942. [CrossRef]
36. Li, P.; Ji, H.; Wang, C.; Zhao, J.; Song, G.; Ding, F.; Wu, J. Optimal Operation of Soft Open Points in Active Distribution Networks Under Three-Phase Unbalanced Conditions. *IEEE Trans. Smart Grid* **2017**, *10*, 380–391. [CrossRef]
37. Bokhari, A.; Alkan, A.; Dogan, R. Experimental Determination of the ZIP Coefficients for Modern Residential, Commercial, and Industrial Loads. *IEEE Trans. Power Deliv.* **2014**, *29*, 1372–1381. [CrossRef]
38. Jardini, J.A.; Tahan, C.M.V.; Gouvea, M.R.; Ahn, S.U.; Figueiredo, F.M. Daily load profiles for residential, commercial and industrial low voltage consumers. *IEEE Trans. Power Deliv.* **2000**, *15*, 375–380. [CrossRef]
39. Initiative Open Energy Data. Available online: Data.openei.org (accessed on 1 October 2021).
40. Renewables.ninja. Available online: https://www.renewables.ninja/ (accessed on 1 October 2021).
41. Li, K.; Cao, X.; Ge, X.; Wang, F.; Lu, X.; Shi, M.; Yin, R.; Mi, Z.; Chang, S. Meta-Heuristic Optimization-Based Two-Stage Residential Load Pattern Clustering Approach Considering Intra-Cluster Compactness and Inter-Cluster Separation. *IEEE Trans. Ind. Appl.* **2020**, *56*, 3375–3384.

42. Yunjie, Z.; Weina, W.; Xiaona, Z.; Yi, L. A cluster validity index for fuzzy clustering. *Inf. Sci.* **2008**, *178*, 1205–1218.
43. Zhou, J.; Zheng, Y.; Xu, Y.; Li, H.; Chen, D. A Heuristic T-S Fuzzy Model for the Pumped-Storage Generator-Motor Using Variable-Length Tree-Seed Algorithm-Based Competitive Agglomeration. *Energies* **2018**, *11*, 944. [CrossRef]
44. Chen, X.; Wu, W.; Zhang, B. Robust Restoration Method for Active Distribution Networks. *IEEE Trans. Power Syst.* **2016**, *31*, 4005–4015. [CrossRef]